3D grain mapping by laboratory X-ray diffraction contrast tomography implemented on a conventional tomography setup

H Fang, R Granger, W Ludwig, Pierre Lhuissier

3D grain mapping by laboratory X-ray diffraction contrast tomography implemented on a conventional tomography setup

H Fang[1, 2], R Granger[1, 3], W Ludwig[2, 4] and P Lhuissier[1]
[1]Université Grenoble Alpes, Grenoble INP, CNRS SIMaP, 38000 Grenoble, France.
[2]European Synchrotron Radiation Facility, BP 220, 38043 Grenoble, France.
[3]Université Grenoble Alpes, Grenoble INP, CNRS 3SR, 38000 Grenoble, France.
[4]Université de Lyon, INSA-Lyon, CNRS MATEIS, 69621 Villeurbanne, France.

E-mail: haixing.fang@grenoble-inp.fr

Abstract. Non-destructive 3D characterization of grain orientations, shapes and sizes, i.e. grain mapping, offers immense opportunities for studying microstructural evolution in polycrystalline materials. In addition to a number of well-established grain mapping techniques available at synchrotron facilities, a polychromatic variant - laboratory diffraction contrast tomography (LabDCT) - using lab-based x-rays, has been developed and commercialized. Yet, the product is bounded to a specific instrument and requires a commercial license, which limits the use on widely available laboratory instruments. To promote the availability of LabDCT, we have developed a grain reconstruction method and implemented it on a conventional X-ray tomography setup at the SIMaP laboratory for LabDCT grain mapping. First, we tested the grain reconstruction algorithm by comparing an input virtual grain structure and a reconstructed volume using the forward simulated diffraction projections from the input structure. Then, we experimentally characterized an AlCu alloy sample using LabDCT and validated the grain mapping result by a grain reconstruction from synchrotron DCT measurement. Last, perspectives on further development of generalizing LabDCT technique on conventional tomography setups are discussed.

1. Introduction

A detailed characterization of grain orientations, morphologies and grain boundary characters is often required for improving properties of metals and alloys. X-ray based grain mapping techniques offer such possibility to characterize 3D grain structures in a non-destructive manner over reasonably large fields-of-view (up to mm^3) and are thus highly complementary to established (surface / thin foil) electron diffraction techniques [1]. A number of grain mapping techniques have been well established at large synchrotron facilities, such as differential aperture X-ray microscopy (DAXM) [2], three-dimensional X-ray diffraction microscopy (3DXRD) [3], diffraction contrast tomography (DCT) [4] and dark-field X-ray microscopy [5]. To broaden the use of grain mapping and overcome the limited access to synchrotron facilities, lab-based diffraction contrast tomography (LabDCT), using a conical polychromatic beam from laboratory source, has been developed [6] and commercialized [7]. The former approach was based on Friedel pair based indexing, followed by tomographic reconstruction and can only deal with moderate number of grains in the illuminated sample volume due to overlap of diffraction spots. The latter product is based on a forward modelling strategy [7], bounded to a specific instrument and requires a commercial license, limiting the use on widely available laboratory instruments.

To promote the availability of LabDCT, we have developed a forward modelling based grain reconstruction method and implemented it on a conventional X-ray tomography setup at the SIMaP laboratory for grain mapping. Multiple algorithms for grain reconstruction have been developed based on

both forward and back calculations. Testing of these algorithms was done by comparing an input virtual grain structure and a reconstructed volume using the forward simulated diffraction projections from the input structure. After the reconstruction algorithms were carefully assessed, we experimentally characterized an AlCu alloy sample using LabDCT and validated the grain reconstruction result by the one from synchrotron DCT measurement. With regard to the flexibility in geometrical configuration and choices of X-ray sources and detectors, we discuss perspectives on further development of generalizing the LabDCT technique on conventional tomography setups.

2. Experimental setup

LabDCT was implemented on a conventional tomography setup (EASYTOM XL Nanofocus tomography manufactured by RX solutions) at the SIMaP laboratory. This tomography instrument has two sources: i) a micro source generating high-flux beam with a source size from 1 to 20 µm, suitable for scanning large objects; ii) a nano source providing a less powerful beam but with a smaller source size, ranging from 0.3 to 3 µm, suitable for scanning small samples to obtain high resolution (Figure 1). For each source there are three modes for tuning the source size (being small, middle and large) according to specific experimental demands. Different combinations of targets (W or Mo) and filaments (W or LaB6) are also available. This setup is adaptable to three detectors: a flat panel detector with 1536×1920 pixels and a pixel pitch of 127 µm, a CCD detector with 2040×2040 pixels and a pixel pitch of 24 µm, and a direct photon counting CdTe detector equipped with two modules. Each module contains 512×402 pixels with a pixel pitch of 62 µm. The large range of choices in sources and detectors offers a flexible solution for different tasks with different samples.

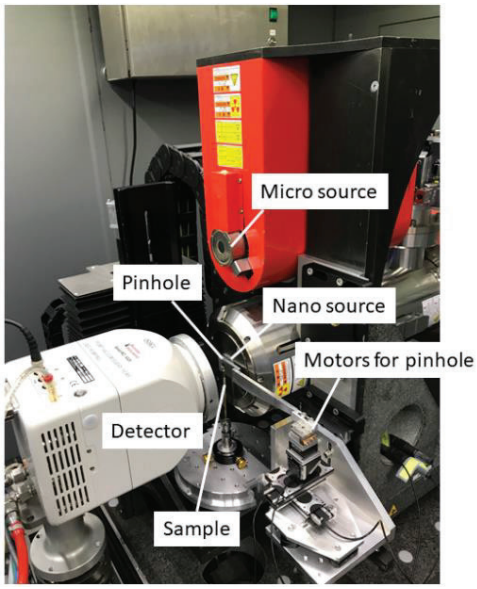

Figure 1. Tomography setup for LabDCT grain mapping.

In diffraction mode for grain mapping, the incoming beam was confined by a pinhole placed in between the sample and the source. As shown in Figure 1, a customized pinhole support was machined and three micro motors (enable movements in *x*, *y* and *z* directions) were used to position the pinhole with a precision of several nanometers. Pinholes with different sizes ranging from Ø50 µm to 2 mm are available for LabDCT measurements. Circular beamstops with different diameters were made of 0.5 mm Pb plates. For diffraction tomography measurement, a beamstop is placed right in front of the detector to block the direct transmitted beam, and thus to enhance diffraction signals recorded by the outer area of the detector. For absorption tomography, the beamstop is removed.

3. Materials and Methods

An AlCu alloy (8 wt.% Cu) sample with a cylindrical diameter of ~650 μm and a height of ~160 μm was cut from a heated treated rod, in which the copper enriched eutectic phase has precipitated at grain boundaries. A conical polychromatic beam emitted from a tungsten target of the nano source (80 kV, 1.3 W and in middle-size mode) was used to illuminate this sample. 2D projections behind the sample were collected by a CCD detector with 2040×2040 pixels and a pixel pitch of 24 μm. The direct transmitted beam was shielded by a beamstop to enhance the diffraction signal. Sample-to-source (L_{ss}) and sample-to-detector (L_{sd}) distances were 6.1 and 52.9 mm, respectively. In total, 121 projections were acquired at a rotation step of 3° and each projection was averaged over 6 frames with an exposure time of 60 s (maximum exposure time allowed for this detector). The experimental parameters selected here were based on exercises to balance the signal-to-noise ratio and the scanning time. A subsequent tomographic scan was also performed to reconstruct a sample shape that serves as a volume mask for grain mapping. The whole diffraction and tomography scan took about 13 h. To reconstruct grain maps, we developed multiple computational efficient methods and the result reported here was obtained using one of these methods (which will be presented in a forthcoming publication). The reconstruction time for this sample was about 6 h using a computing node equipped with a NVIDIA Tesla V100-PCIE-32GB GPU on the ESRF cluster.

This sample was also characterized by synchrotron DCT at beamline ID11 of European Synchrotron Radiation Facility (ESRF). A parallel monochromatic beam with an energy of 43.6 keV was used to illuminate the sample. Transmitted diffraction signals were recorded by a sCMOS (Andor Marana) camera with 2048×2048 pixels, coupled to a 10 μm thickness transparent luminescent screen via a 7.5× objective lens, resulting in an effective pixel size of 1.22 μm. The distance between the rotation axis and the detector was 11 mm. A DCT scan contains 3600 equally spaced projections over 360° sample rotation. Exposure time for each projection was 0.1 s and a total scan took about 10 min. Subsequent grain reconstruction was performed using the method described in [4, 8]. The obtained grain map was verified by the good agreement with the tomography volume, where the Cu-enriched eutectic phase was resolved at grain boundaries. Therefore, we directly use this grain map to check the grain structure reconstructed by LabDCT.

To test the grain reconstruction algorithm for LabDCT, simulated projections using a forward projection model [9] were created from a virtual Fe grain structure, containing 6 grains with an average size of 100 μm in a cylindrical volume (a diameter of 150 μm and a height of 300 μm). The simulations were performed in the same conditions as the experiment described above. A grain structure was reconstructed based on the simulated projections. The grain reconstruction time was about 20 min using the same computer as described above.

4. Results and discussion

4.1. Reconstruction of the virtual sample

Figure 2 compares grain structures between the ground truth input and the reconstructed result. In total 6 grains have been reconstructed, which is the same as the input. 3D visualizations (Figure 2a and b) show that all the reconstructed grains are very similar in shape with respect to the input. Examination on 2D slices show that grain boundary positions are largely coincident (Figure 2c). 95% of the voxels are fully matched and more than 98% deviate no more than 2 pixels. The maximum deviation is found to be 4 pixels only. As shown in Figure 2d, comparison of grain size confirms that the grains were accurately reconstructed and the relative grain size difference is 1.7% ± 0.8% (mean and standard deviation). The disorientation of grain pairs between the input and the reconstructed grain maps is 0.05 ± 0.01°. The grain center-of-mass is 0.89 ± 0.46 pixels. All these numbers indicate that the reconstruction algorithm performs well and the reconstructed grain map is in very good agreement with the input one.

To further assess the performance of the reconstruction algorithm, we used the forward projection model to check the positions and the shapes of the spots from the reconstructed grain map on the initially simulated LabDCT projections, i.e. regarded as “experimental” projection. Figure 3a shows that the outlines of the simulated spots match very well with the “experimental” ones. To quantify the difference, we calculated the difference in Euclidian distance of center-of-mass for each spot pair (Δ_{dis}). Statistics of the spot pairs

present in all the 121 projections are summarized in Figure 3b. The figure shows that $\Delta_{dis} = 1.7 \pm 1.3$ pixels, approximately 2 times the deviation of grain centroids.

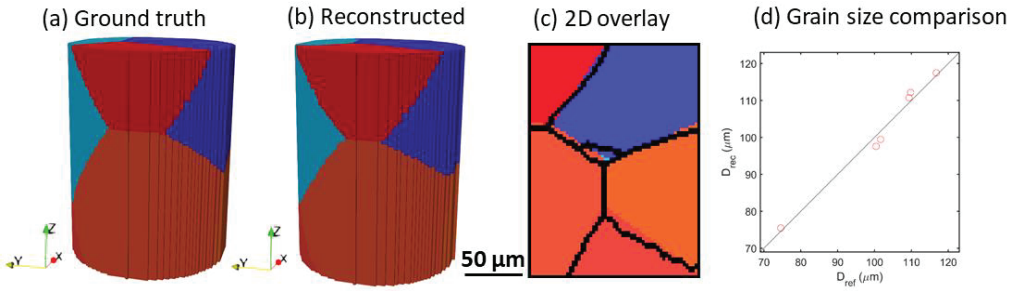

Figure 2. Comparison of reconstructed grain structure by LabDCT with the ground truth input. (a) Ground truth input and (b) reconstructed structures visualized in 3D; (c) overlay of grain boundaries in the reconstructed grain map onto the corresponding XZ slice of the ground truth; (d) grain size comparison between the ground truth and the LabDCT reconstruction. Grains are colored in IPF-Z direction. Voxel size is 2.5 µm.

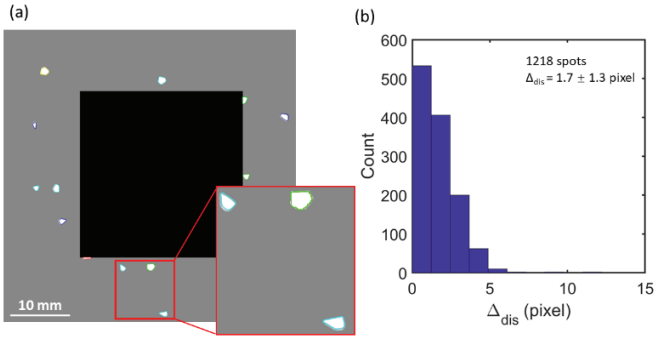

Figure 3. Verification by forward simulated spots. (a) Overlay of forward spots from the reconstructed grain structure onto the LabDCT projection simulated for the initial ground truth input; (b) statistics of Δ_{dis} between the reconstructed and the input structures. Outlines of the forward projected spots are colored according to {*hkl*} families: red-{011}; green-{002}; blue-{112}; yellow-{022}; cyan-{013}.

4.2. Reconstruction of the experimental AlCu alloy sample

Figure 4 shows grain maps reconstructed from the synchrotron radiation DCT (SR-DCT) and the LabDCT measurements. A full volumetric grain map was reconstructed from SR-DCT, which contains 329 grains with an average grain size of 52.5 ± 20.5 µm. At the time of the LabDCT measurement performed, the current on the target of the X-ray source was rather limited, thereby a relatively low flux was used for scanning this sample. As a result, diffraction signals from relatively small grains (mostly < 40 µm) could not be distinguished and properly segmented from the background noise in the projection images. To exclude the effect of the undetected signals on the comparison of grain maps between SR-DCT and LabDCT, we used the forward model to compute values of two parameters for each grain centroid voxel: 1) completeness (*Comp*), i.e. the number of intersected spots between forward simulation and experiment divided by the theoretically expected number of spots on the detector; 2) median distance (D_{med}), median value of distances between each forward simulated spot and its nearest experimental one. During the LabDCT reconstruction, indexing of voxel orientation was accepted only when the voxel has $Comp \geq 0.3$ as well as $D_{med} < 20$ pixels. Therefore, the same condition was used to filter the grain map of SR-DCT and a partial map was thus obtained as shown in Figure 4b.

Figure 4c shows the grain map reconstructed from LabDCT. Compared to Figure 4b, the same number of grains was obtained and each grain has similar shapes and locations as its counterpart in SR-DCT. By pairing all the grains, we compared the disorientation and the center-of-mass distance between corresponding grains. Results show that the disorientation of grain pairs is 0.06 ± 0.03° and the grain center-of-mass distance is 3.96 ± 1.35 pixels. This is less well, compared to the result of the reconstruction for the synthetic dataset described above. Since the diffraction signals were relatively low because of the low flux, a complete grain indexing and reconstruction cannot be obtained for this sample volume. Additionally,

many spots can be under-segmented, restricting the proper voxel growth of the corresponding grains. Examples of these grains are indicated by the red arrows in Figure 4c, showing that they are significantly smaller compared to their counter parts in Figure 4b. The difference in average grain size further confirms a high degree of spot under-segmentation, where the average grain size is 75.9 ± 8.8 µm for the filtered grain map of SR-DCT and it is 64.7 ± 19.7 µm for the grain map of LabDCT.

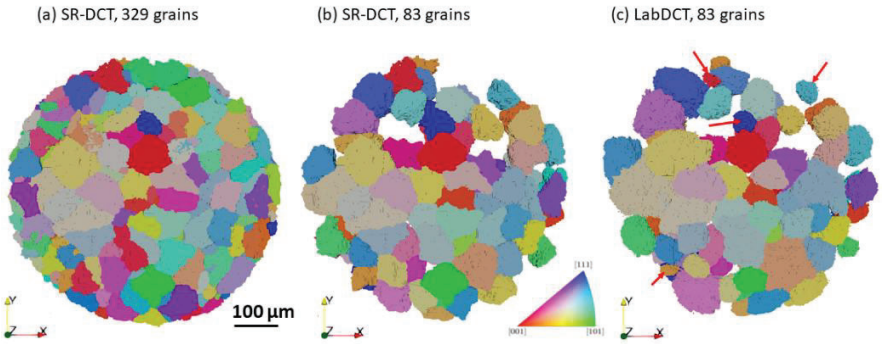

Figure 4. Grain maps reconstructed from synchrotron radiation DCT (SR-DCT) and LabDCT for an AlCu alloy sample. (a) full grain map from SR-DCT contains 329 grains; (b) a filtered grain map contains 83 grains, whose completeness (*Comp*) ≥ 0.3 and median distance (D_{med}) < 20 pixels based on forward calculation result on the LabDCT projections; (c) grain map reconstructed from LabDCT contains 83 grains with *Comp* ≥ 0.3 and D_{med} < 20 pixels. Grains are colored in IPF-Z direction. Voxel size is 2.7 µm.

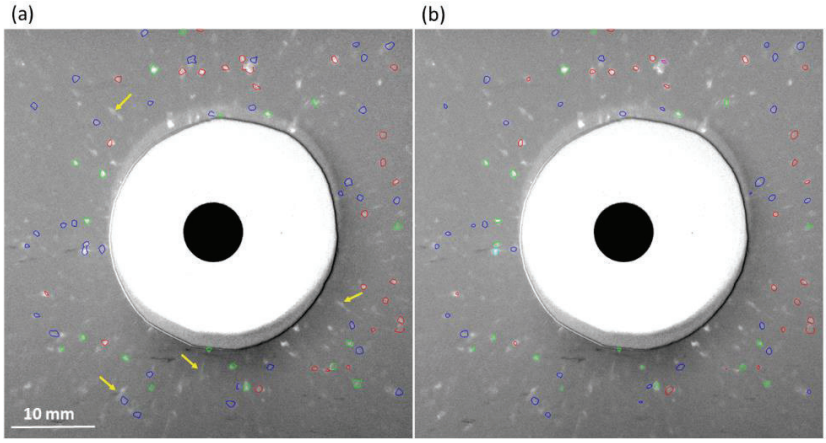

Figure 5. Overlay of forward projected spots from the reconstructed (a) SR-DCT and (b) LabDCT grain maps onto the LabDCT projections. Yellow arrows indicate examples of streaking spots. Outlines of the forward spots are colored according to {*hkl*} families: red-{111}; green-{002}; blue-{022}.

To verify both reconstructions, we computed the diffraction spots using the forward projection model and overlaid them onto the experimental projection. As shown in Figure 5a and b, most of the forward spots superimposed well onto experimental spots. Some may slightly shift while some others may be too big or too small compared to their overlaid experimental spots. Statistics of Δ_{dis} for more than 1400 spots for all the 83 grains show that Δ_{dis} = 5.2 ± 3.1 pixels for SR-DCT and Δ_{dis} = 5.7 ± 3.3 pixels for LabDCT. This suggests that the LabDCT reconstruction is only slightly less performed compared to SR-DCT. The reason for not having a smaller value of Δ_{dis} for SR-DCT is that some grains may contain non-negligible strain as indicated by some streaky spots (see Figure 5). Although the lattice strain was not considered during SR-DCT reconstruction, the quality of the SR-DCT reconstruction was less affected compared to LabDCT as a monochromatic parallel beam was used for the SR-DCT measurement.

4.3. Discussion

The comparisons of different grain maps demonstrate that grain mapping by LabDCT has been implemented successfully on a conventional laboratory instrument and a computational efficient grain reconstruction method has been established. Notably, this method is general and it can be applied to reconstruct grain maps for diffraction data acquired on other tomography instruments in both Laue-focusing and non-Laue-focusing geometries.

The experimental result also shows that a weak X-ray beam ultimately limits the capability of LabDCT to reconstruct small grains. As a result of unsuccessful reconstruction for small grains, shape reconstruction for already-indexed grains may be affected and may not be accurate due to over-growth. Therefore, increasing the photon flux as well as higher detective quantum efficiency of the detector system are very important to further improve the performance of LabDCT in addition to improvements in spot segmentation and reconstruction algorithm [10, 11]. To these aims, we suggest the following measures: 1) allow higher current on the target of the source using thicker material for the anode or improving the heat conduction around the target; 2) use direct photon counting detectors such as the CdTe 'color' detectors, which are expected to produce low background noise, have better detective quantum efficiency at high X-ray energies and offer the capability to define an X-ray energy range for detecting signals. On the other hand, there is a need to reduce scanning time for LabDCT experiments, thereby enabling 4D (space + time) characterization. This requires fast counting detectors, such as flat panel with large pixel pitch or direct photon counting detector equipped with CMOS chip, as well as a generous geometrical constraint for optimizing different settings of L_{sd} considering the area and the pixel pitch of each different detectors.

5. Conclusions

In this study, we demonstrate that grain mapping by LabDCT was made available on a conventional tomography setup at the SIMaP laboratory. A computational efficient grain reconstruction algorithm has been developed and a pipeline to reconstruct grain maps has been established. Verification by a virtual Fe sample indicates a good performance of the current method. The differences in disorientation and positions of grain center-of-mass are $0.05 \pm 0.01°$ and 0.89 ± 0.46 pixels, respectively, and the relative grain size difference is $1.7\% \pm 0.8\%$. The comparison of grain maps for an AlCu alloy sample reconstructed from SR-DCT and LabDCT further validates the reconstruction method. Suggestions for further developing the LabDCT technique towards better detection limit and faster acquisition were presented.

Acknowledgements

This work is part of the project Advanced Laboratory X-ray Microtomography funded by the Agence Nationale de la Recherche (ANR-18-CE42-0005).

References

[1] Shahani A J, Xiao X, Lauridsen E M and Voorhees P W 2020 *Mater. Res. Lett.* **8** 462
[2] Larson B C, Yang W, Ice G E, Budai J D and Tischler J Z 2002 *Nature* **415** 887
[3] Poulsen H F 2020 *Curr. Opin. Solid. St. Mater. Sci.* **24** 100820
[4] Ludwig W, Schmidt S, Lauridsen E M and Poulsen H F 2008 *J. Appl. Cryst.* **41** 302
[5] Simons H, King A, Ludwig W, Detlefs C, Pantleon W, Schmidt S, Stöhr F, Snigireva I, Snigirev A and Poulsen H F 2015 *Nature Comm*. **6** 6098
[6] King A, Reischig P, Adrien J and Ludwig W 2013 *J. Appl. Cryst*. **46** 1734
[7] Bachmann F, Bale H, Gueninchault N, Holzner C and Lauridsen E M 2019 *J. Appl. Cryst.* **52** 643
[8] Reischig P, King A, Nervo L, Viganó N, Guilhem Y, Palenstijn W J, Batenburg K J, Preuss M and Ludwig W 2013 *J. Appl. Cryst*. **46** 297
[9] Fang H, Juul Jensen D and Zhang Y 2020 *Acta Cryst.* A **76** 652
[10] Fang H, Juul Jensen D and Zhang Y 2021 *IUCrJ* **8** 559
[11] Fang H, Hovad H, Zhang Y, Clemmensen L K H, Kjaer Ersbøll and Juul Jensen D 2021 *IUCrJ* **8** 719